THE ASTROPHYSICAL JOURNAL, 462:316–325, 1996 May 1


# THE LOCAL DIRECTION AND CURVATURE OF THE GALACTIC MAGNETIC FIELD DERIVED FROM STARLIGHT POLARIZATION

CARL HEILES
Astronomy Department, University of California, Berkeley, CA 94720; cheiles@astro.berkeley.edu.
*Received 1995 July 28; accepted 1995 November 9*

## ABSTRACT

We use the Mathewson & Ford compilation of starlight polarization data to derive the local direction and curvature of the Galactic magnetic field lines. We find the field lines are spirals, with a local radius of curvature $8.8 \pm 1.8$ kpc and a local inclination angle $i = 7.^\circ2 \pm 4.^\circ1$. Despite these apparently large errors, we show that with high statistical confidence our results are inconsistent with those derived from pulsar data by Rand & Lyne, with a concentric-circle model, and with a spiral-arm model having inclination $i = 12.^\circ5$ (the standard value for the Galaxy). In external galaxies, the field lines follow the spiral pattern closely. Unless the magnetic field pattern of the Galaxy is unique, we must invoke local distortions of the spiral pattern or the field lines; such distortions might conceivably be Galactic in scale and related to the field reversal that occurs just inside the solar circle.

*Subject headings:* ISM: magnetic fields — polarization

## 1. INTRODUCTION

The direction and strength of the uniform component of the Galactic magnetic field are important for understanding its origin and evolution, its effect on interstellar gas-dynamics, and other astrophysical issues. The best current model for the field is based on the detailed analysis of pulsar rotation measures (RMs) and dispersion measures (DMs). Rand & Lyne (1994, hereafter RL) find that the local field strength is $1.4 \pm 0.2$ $\mu$G and the direction is $l_0 = 88^\circ \pm 5^\circ$. RL favor field lines that are circular and centered at the Galactic center. RL find that the field undergoes one or more reversals. The nearest one, for which the observational evidence is indisputable, lies about 0.4 kpc inside the solar circle.

If this model of concentric circular field lines for the Galaxy is correct, then the Galaxy differs from external spiral galaxies, in which the field lines closely follow the spiral arms (see reviews by Beck 1993 and Heiles 1995). Furthermore, as emphasized by Heiles (1995), the pulsar results do not demand interpretation in terms of a circular field, because most of the pulsar data are restricted to Galactic quadrant 1; in his opinion, a spiral field seems to be as likely as a circular field, although he has not performed an independent analysis of the pulsar data.

In the present paper we derive the local direction and curvature of the field lines from the polarization of starlight,[1] which historically was the first observational indication of the existence of the Galactic magnetic field. In a second analysis, currently in progress, we examine the random component of the field; Heiles (1966) provides preliminary results. The most recent major large-scale data set remains the compilation of different observers for both the northern and southern skies by Mathewson & Ford (1970, hereafter MF), which is impressively large with nearly 7000 stars. Even though this data set is old, it is outstanding in two respects. First, the polarization data are essentially free from systematic errors because there is excellent agreement among the many stars which were duplicated by the observers; also, some of the observers used telescopes specifically designed for polarization work, with the entire telescope tube and mirror free to rotate around its axis. Second, the data set contains not only accurate polarization measurements but also estimates of extinction and distance.

Investigations of the uniform component of the Galactic magnetic field are complicated by the random component of the field, whose strength exceeds that of the uniform component. The previous analysis of pulsar data modeled by Rand & Kulkarni (1989) contains a model for field fluctuations. Field fluctuations are large and depend on the assumed scale length; Rand & Kulkarni find that a single scale length is not consistent with the results. More recent work by Ohno & Shibata (1993) finds the random component to be $\sim 5$ $\mu$G, roughly independent of scale length, and furthermore their Figure 6, which compares the $\chi^2$ for three assumed scale lengths, favors a scale length for fluctuations of $\sim 100$ pc. Heiles (1995) reviews these matters and concludes that both pulsar data and synchrotron data indicate a random component in the solar vicinity $\sim 5$ $\mu$G. The presence of large fluctuations with large scale length is also deduced from studies of starlight polarization (Jones, Klebe, & Dickey 1992). Thus, the major part of the field strength comes from the random component. This means that the "cosmic scatter" is large and underscores the necessity to investigate the uniform component in as many ways as possible.

The direction of the uniform field is indicated by the pattern of the stellar polarization "vectors."[2] For a uniform magnetic field, the optical polarization vectors are parallel to the direction of field lines projected onto the plane of the sky. Thus, when looking along the field lines, the polarization vectors appear to "recede into the distance." This convergence effect is similar to that observed by standing on a railroad track and looking down the tracks. Heiles (1976)

[1] In fact, the starlight polarization tells nothing about the sign of the field, so it only provides the field *orientation*. In the present paper we resolve the ambiguity in sign by using the pulsar results, which are very well established (see RL). Then, sacrificing precision for simplicity, we speak of the starlight polarization alone as providing the field "direction."

[2] Of course, they are not true vectors. However, for the sake of simplicity, we shall refer to them as vectors without the quotation marks.

noted, from visual inspection of MF's map, that the convergence points appear near $l \sim 80°$ and 260°, distinctly (but perhaps not significantly) different from the pulsar direction (which, in 1976, was $l \sim 94°$).

Below, we will find that our detailed analysis of the starlight data indicate a direction which is distinctly (and significantly) different from RL's pulsar direction. Furthermore, we find that the local lines are definitely inconsistent with two models that one might reasonably expect for the field lines: concentric circular field lines, and spiral field lines with the standard Galactic 12°.5 pitch angle. Instead, the local field line pattern lies roughly between these two.

We will argue that the starlight data are far superior to the pulsar data for determining the local *direction* of the field. However, we emphasize that the starlight data provide no information on field *strength*. The only indications of strength come from pulsar data and the synchrotron volume emissivity. Thus, while the current paper puts forth a new result for the pattern of field lines that should, we believe, supplant RL's pulsar result, it says nothing about the field strength.

## 2. THE LEAST-SQUARES FIT: THE MODEL AND THE TECHNIQUE

### 2.1. *The Model*

Let us suppose that all grains are alike in the following two senses: (1) that the alignment is such that the polarization of extincted starlight is parallel to the magnetic field, i.e., $\theta_p = \theta_B$, where $\theta$ is the direction in the plane of the sky, the subscript $p$ means the observed polarization, and the subscript $B$ means the magnetic field; and (2) that the ratio of the polarization produced perpendicular to the field to the extinction is constant, i.e.,

$$\frac{p_\perp}{A_V} = p_A = \text{constant} . \tag{1}$$

Physically, these assumptions are equivalent to assuming that all grains are alike and that all are perfectly aligned in the magnetic field. This is consistent with observation: dust grains seem to always be well aligned (Jones et al. 1992). Furthermore, let us suppose that the magnetic field is uniform and points in direction $\phi_0$ (toward the "magnetic pole"). For this case, the polarization vectors point toward the magnetic pole and $p$ is linearly proportional to the product of extinction and the sine of the angle between the field and the line of sight:

$$p = p_\perp \sin (\phi - \phi_0) , \tag{2}$$

where $\phi$ is the direction of the line of sight. Returning to the railroad analogy, the tracks recede into the distance toward direction $\phi_0$; the polarization vectors point along the tracks, with the magnitude proportional to the apparent distance along the tracks between the ties.

We express the polarization by $\Delta l_B$ and $\Delta b_B$, its projection and length along the two directions of Galactic coordinates. Let the uniform field point toward $(l_0, b_0)$; then we have

$$\Delta l_B = p_\perp \sin (l - l_0) \frac{\cos b_0}{\cos b} \tag{3a}$$

and

$$\Delta b_B = p_\perp (\sin b \cos b_0 \cos (l - l_0) - \cos b \sin b_0) . \tag{3b}$$

Of course, these lead to

$$\theta_p = \tan^{-1} \frac{\Delta l_B}{\Delta b_B} \tag{4a}$$

and

$$p = p_\perp \sqrt{\Delta b_B^2 + (\Delta l_B \cos b)^2} . \tag{4b}$$

In the above equation and in the remainder of this paper, the angle $\theta$ is the position angle relative to Galactic coordinates as defined by MF: it is zero when the polarization vector points toward $b = 90°$ and increases toward increasing $l$.

### 2.2. *The Technique*

We perform the least-squares fit in two ways. In one, we ignored the extinction $A_V$ and solved for the mean polarization $p_\perp$ in equation (1). In the other, we included the extinction and solved for the mean polarization per unit extinction, $p_A$. Both methods produced closely similar results for the field direction. We chose the former method to avoid possible errors in the extinctions, which depend on the details of stellar classification. The errors in the polarization data are essentially random and depend mainly on the signal-to-noise ratio, which in turn depends only on the apparent brightness of the star and the integration time. In this paper, all polarizations $p$ are expressed in percent.

To perform the least-squares fit, we define the observed Stokes parameters for each star (denoted by $i$) $Q_{\text{obs},i}$ and $U_{\text{obs},i}$ with respect to the Galactic plane as

$$Q_{\text{obs},i} = p_i \cos (2\theta_{p,i}) , \tag{5a}$$

$$U_{\text{obs},i} = p_i \sin (2\theta_{p,i}) , \tag{5b}$$

where $p_i$ is the star's observed percentage polarization and $\theta_{p,i}$ its polarization angle. There are equivalent definitions for the model-predicted values derived from equations (4), which we denote $Q_{\text{thy},i}$ and $U_{\text{thy},i}$.

The least-squares fit involves nonlinear terms in $l_0$ and $b_0$, together with a linear term in $p_\perp$. We use a combination of the "brute force" iterative approach for $l_0$ and $b_0$ and a standard fit for $p_\perp$. Specifically, we assume values for an $(l_0, b_0)$ pair and perform a conventional least-squares solution for $p_\perp$. Then we calculate the sum of the squares of the residuals of each star $\sigma_i^2 = (Q_{\text{obs},i} - Q_{\text{thy},i})^2 + (U_{\text{obs},i} - U_{\text{thy},i})^2$ and obtain the mean square residual $\sigma^2$. We repeat this procedure for various $(l_0, b_0)$ pairs and search for the minimum in $\sigma^2$. We discarded any star for which $\sigma_i^2 \geq 9.0\sigma^2$, which affected only a very small number of stars. We searched for the minimum, first using the subroutine AMOEBA in Press et al. (1989, chap. 10.4), and then visually inspecting the behavior of $\sigma^2$ in the vicinity of the minimum. To determine the formal least-squares error of the derived parameter $p_\perp$ we accepted the conventionally-defined error in a linear single-parameter least-squares fit.

To determine the formal errors of $l_0$ and $b_0$ we used the technique outlined in Press et al. (1989, chap. 14.5); for our case, the covariance matrix is such that this procedure is equivalent to the simpler equation (11-31) in Bevington (1969). In the vicinity of the minimum at $(l_0, b_0)$, $\sigma^2$ is a paraboloidal function of $l_0$ and $b_0$. The curvature of the paraboloid depends on direction, as expressed in the curvature matrix $[\alpha]$, or its reciprocal, the covariance matrix $[C]$. We found that the curvature in $l$ was always significantly less than that in $b$, and for all practical purposes the prin-

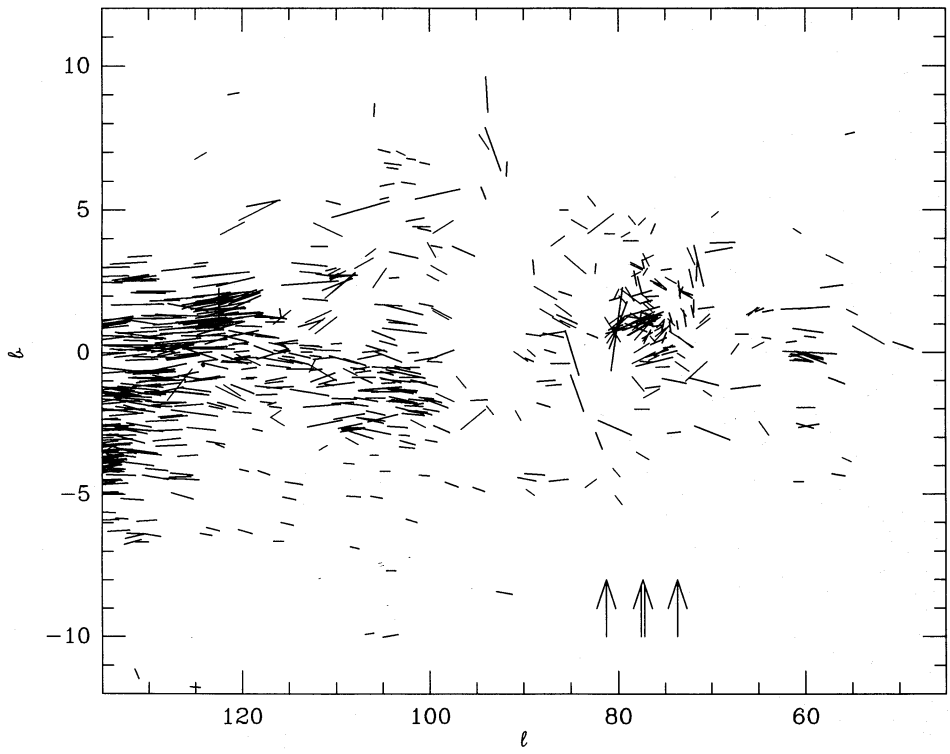


FIG. 1a

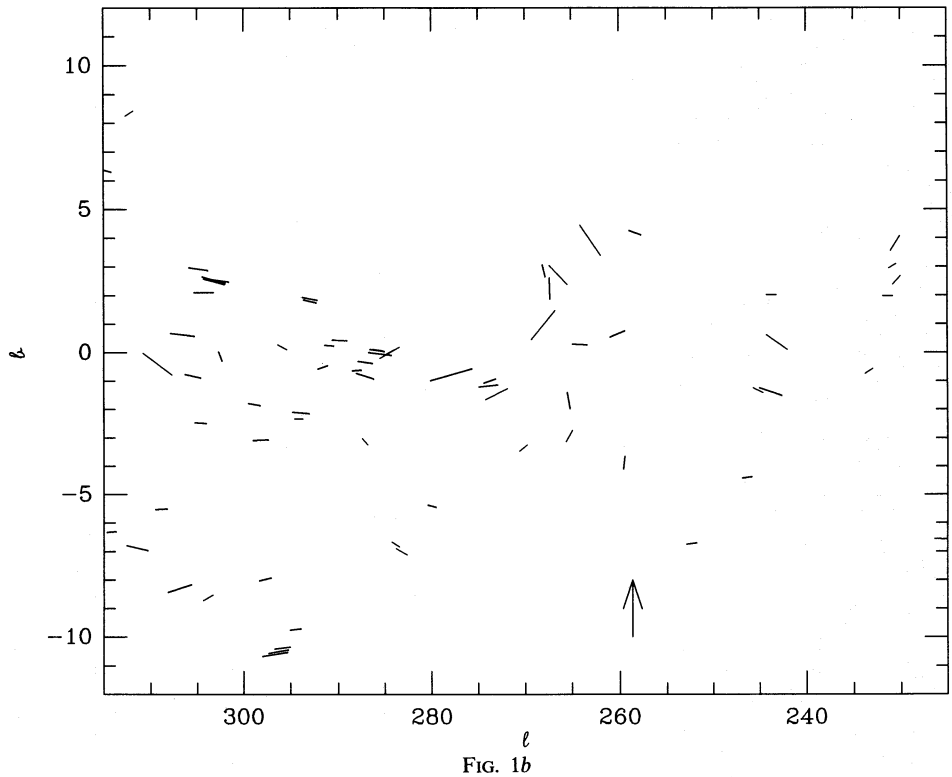


FIG. 1b

FIG. 1.—(*a*) Stellar polarization vectors for our quadrant 1. There are 734 stars; all have $45° < l < 135°$, $-12° < b < 12°$, $p \geq 1\%$. The single arrows show the two values of $l_0$ for the double minimum of our least-squares fit, and the double arrow shows the adopted $l_0$ (§ 3). (*b*) Stellar polarization vectors for our quadrant 3. There are 73 stars; all have $225° < l < 315°$, $-12° < b < 12°$, $p \geq 1\%$. The arrow shows $l_0$ for our last-squares fit (§ 3).

cipal axes of all curvature matrices were parallel to the Galactic coordinates $l$ and $b$; this allows us to specify the errors in the conventional way, as independent 1 $\sigma$ errors in $l_0$ and $b_0$. We denote the 1 $\sigma$ error in these parameters, say $l_0$, by the usual symbol $\sigma_{l_0}$: it is defined as the incremental angle from $l_0$ at which $\sigma^2$ increases from its minimum value by the fractional amount $1/(N-M)$, where $N$ is the number of stars and $M$ the number of fitted parameters; here $M = 3$.

However, we found that there is an additional complication for the direction $l$. In "quadrant 1" (defined below), many sets of data produced not just one but *two* minima separated by $\sim 8\overset{\circ}{.}0$. This is not too surprising, because the data (Fig. 1*a*) give the visual impression that the

vectors converge over a broad $\sim 10°$ wide interval in $l$. For these double-minimum cases our quoted results for $l_0$ and $b_0$ are the average of the two solutions. We discuss the double-minimum situation to detail below in § 4.1.

### 2.3. *Selection of Stars by Position*

As discussed above, the optical polarization vectors converge in the direction of the field lines. MF's classic, well-known map of starlight polarization exhibits several places near $b = 0°$ where the vectors appear to converge and we look along the field lines. The most obvious is near $l \sim 30°$. However, this is the direction where the North Polar Spur (NPS) meets the Galactic plane. The NPS is a nearby supershell (e.g., Heiles et al. 1980) whose wall is very well delineated by the polarization vectors. This is an example of a major, nearby perturbation in the field, a "magnetic bubble" (Vallée 1993); it also has a major effect on pulsar RMs. As a strong perturbation, it is both irrelevant and undesirable for determining the properties of the Galactic field. The NPS is 120° in diameter, which means that it dominates the magnetic field toward the whole inner Galaxy. Even distant stars have their light polarized significantly by this perturbation. Therefore, stars toward the Galactic interior should not be included in our fit.

MF's map shows two other directions where the vectors converge; these are in very rough agreement with pulsar results, but more accurately appear to be near $l \sim 80°$ and 260°. MF's maps exhibit no obvious perturbations near these directions. However, MF's maps do exhibit a second noticeable perturbation in the vector pattern appearing near $l \sim 210°$, roughly toward the direction of Orion. This suggests that regions of intense star formation are likely to perturb the field, and leads us to consider with disfavor the regions near Taurus and Perseus, i.e., $150° \lesssim l \lesssim 200°$. Therefore, we exclude stars toward the Galactic exterior.

We are left with stars located near the directions toward and from which the field points. This is fortunate for our purposes, because it is just such stars whose polarization is most sensitive to the field direction. In fact, including stars located very far in angle from the field direction cannot increase the accuracy of a least-squares fit, because the polarization vectors of such stars are insensitive to the field direction.

We include in our fit two 90° slices in $l$ centered on $l = 90°$ and 270°. We denote these two slices "quadrant 1" and "quadrant 3," respectively. We restrict the latitude coverage to $|b| < 12°$ so as to exclude stars as high $|z|$; such stars are irrelevant for the large-scale Galactic field because it lies roughly in the Galactic plane.

## 3. THE RESULTS FOR A FIELD WITH ZERO CURVATURE

We experimented with many trial least-squares fits in quadrants 1 and 3 for stars binned in distance, polarization, and $A_V$. The results are insensitive to the binning except for distance, as discussed below (§ 4). We first neglect the distance dependence and concentrate our discussion on stars binned in polarization.

In quadrant 1, stars with small polarization ($p_i < 1\%$) provide $(l_0, b_0) \approx (42°, 0°)$, which is totally discrepant with the results from $p_i > 1\%$. This is commensurate with our finding that stars with small distances (<500 pc) in both quadrants 1 and 3 also provide discrepant results. On the contrary, all bins with stars having $p_i > 1\%$ provide consistent results. Therefore, for this first fit we reject all stars for which $p_i < 1\%$.

Figure 1 exhibits the polarizations of the stars we included in quadrants 1 and 3. For quadrant 1, the convergence of the vectors near $l \sim 77°$ is clear, and with some effort one can imagine two points of convergence as discussed in § 4.1 and illustrated by the arrows on Figure 1*a*. For quadrant 3 there are many fewer stars and the solution is not so evident to the eye, which is reflected in a large formal error for the least-squares fits.

Table 1 presents the results of the fits. For quadrant 3, we obtain $(l_0, b_0) = (78.^\circ7 \pm 5.^\circ7, 2.^\circ1 \pm 2.^\circ5)$. For quadrant 1, the mean of the two solutions is $(l_0, b_0) = (77.^\circ2 \pm 1.^\circ9, 0.^\circ4 \pm 0.^\circ5)$. For the combination of quadrants 1 and 3, the mean of the two solutions is almost identical to that for quadrant 1, with $(l_0, b_0) = (77.^\circ2 \pm 1.^\circ8, 0.^\circ4 \pm 0.^\circ5)$; this agreement is unsurprising, because the total solution is dominated by quadrant 1, which has 10 times more stars than quadrant 3.

The fits also provide $p_\perp$, the mean polarization that would be observed if the magnetic field were perpendicular to the line of sight (eq. [1]). For quadrants 1 and 3, we have $p_\perp = 4.64$ and 2.50; stars in quadrant 1 are polarized 1.9 times those in quadrant 3. Table 1 also presents the mean distance and extinction of the stars, and shows that the increased polarization occurs because the quadrant 1 stars have both larger extinction per unit distance and also larger distances than the quadrant 3 stars. The two quadrants have almost the same values of $p_A$ (eq. [1]). The lower mean extinction per unit distance for stars in quadrant 3 may be related to the long distance to the wall of the "local bubble" in the lower longitude half of quadrant 3 (Paresce 1984).

For the direction of the local field assuming zero curvature, we adopt the quadrant 1 + 3 solution from Table 1:

$$(l_0, b_0) = (77.^\circ4 \pm 1.^\circ8, 0.^\circ4 \pm 0.^\circ5)\,. \quad (6)$$

## 4. THE LOCAL CURVATURE OF THE GALACTIC FIELD

### 4.1. *The Double Minimum and Its Behavior with Distance*

For many of our trial fits involving our quadrant 1, we obtained not just one but two minima, separated by $\sim 8°$. One minimum was always smaller than the other by an amount that is statistically significant, but not excessively

TABLE 1

RESULTS FOR $p > 1\%$, $|b| < 12°$

| Quadrant | ⟨Distance⟩ (kpc) | $\langle A_V \rangle$ (mag) | $l_0$ | $b_0$ | $p_\perp$ | $\sigma^2$ | $N$ |
|---|---|---|---|---|---|---|---|
| 1[a] ..... | 2.2 | 2.2 | $77.2 \pm 1.9$ | $0.4 \pm 0.5$ | $4.64 \pm 0.12$ | 3.79 | 734 |
| 3 ..... | 1.6 | 1.3 | $78.7 \pm 5.7$ | $2.1 \pm 2.5$ | $2.50 \pm 0.39$ | 2.92 | 73 |
| 1 + 3[a]..... | 2.1 | 2.1 | $77.4 \pm 1.8$ | $0.4 \pm 0.5$ | $4.48 \pm 0.12$ | 3.88 | 807 |

[a] For quadrants 1 and 1 + 3, $\sigma^2$ had a double minimum. The $l_0$ and $b_0$ quoted are the averages of the values at the two minima. The two solutions are, for quadrant 1, $(l_0, b_0) = (73.^\circ1, 0.^\circ7)$ and $(81.^\circ3, 0.^\circ0)$; and for quadrant 1 + 3, $(l_0, b_0) = (73.^\circ7, 0.^\circ7)$ and $(81.^\circ1, 0.^\circ1)$.

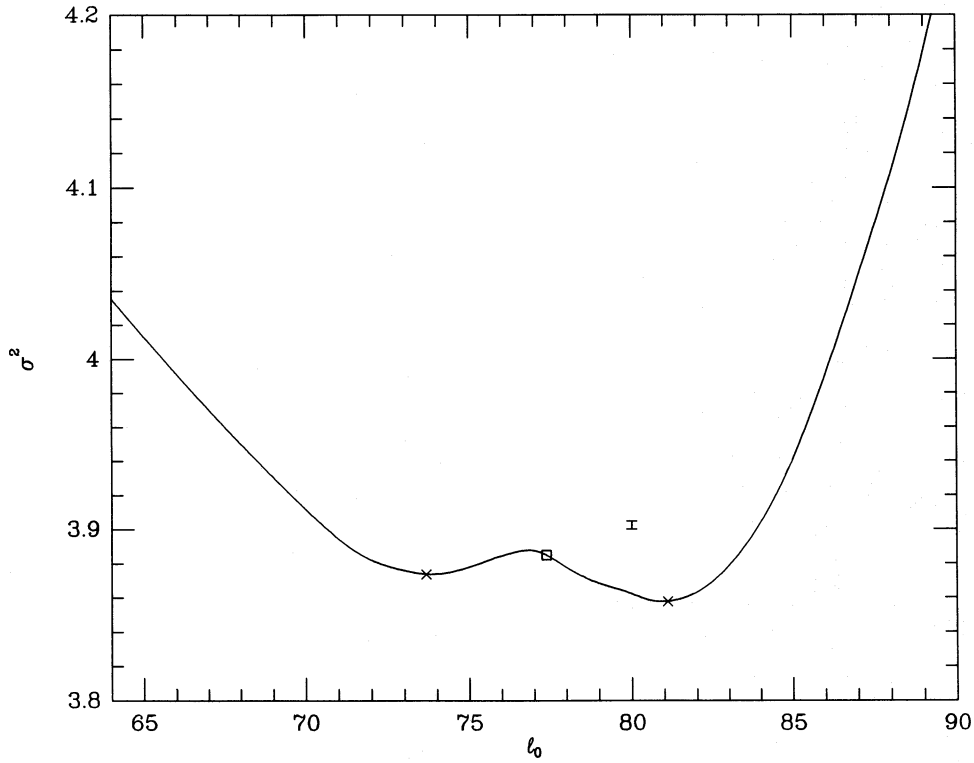


FIG. 2.—Mean square residual $\sigma^2$ vs. $l_0$ for the quadrant 1 + 3 solution. We vary $b_0$ linearly with $l_0$, so that the curve accurately samples the two individual minima (*crosses*) and the adopted Table 1 solution (*square*). If there were only a single minimum, then the "error bar" would represent the vertical distance from the minimum $\sigma^2$ that defines $\sigma_{l_0}$, the 1 $\sigma$ error in $l$.

so. Figure 2 illustrates this behavior by showing $\sigma^2$ versus $l_0$ for the quadrant 1 + 3 solution; we vary $b_0$ linearly with $l_0$, so that the curve samples the two individual minima and the adopted Table 1 solution, in order to avoid having to present a less comprehensible contour plot. The square in Figure 2 represents our adopted Table 1 solution $(l_0, b_0) = (77.^\circ4, 0.^\circ4)$, and the crosses represent the double minima, which were $(73.^\circ7, 0.^\circ7)$ and $(81.^\circ1, 0.^\circ1)$.

The two minima are $\sigma^2 = 3.874$ and 3.858, the difference being 0.016; with 807 stars in the sample, the 1 $\sigma$ error level (illustrated by the "error bar" in Fig. 2) is 3.85/804 = 0.00479, 3.4 times smaller. From the formal statistical standpoint, this means that the lower minimum represents a significantly better fit. Nevertheless, the solution is not robust at this level because the details of the behavior of $\sigma^2$ depend on the sample of stars included. Consequently, one might wish to regard the formal error in $l_0$ as an underrepresentation of the true error. However, it is more correct to regard the model as an inadequate description of the data.

In particular, the reason for the double minimum becomes clear by binning the stars in *distance*. We accept all polarizations, including $p_i < 1\%$, and bin the data into three distance intervals: 0.5–1.0 kpc ("near"), 1.0–2.0 kpc ("middle"), and above 2 kpc ("far"). Figure 3 shows the data for the three distance intervals. Table 2 presents the numerical results, and Figure 4 shows the behaviors of $\sigma^2$ (normalized to their minimum values) for the three intervals. The middle interval exhibits both minima. In contrast, both the near and far intervals exhibit only *single* well-defined minima with smaller errors. There is a smooth decrease of $l_0$ with distance: going from near to far, $l_0$ goes from $84.^\circ8 + 2.^\circ5$ to $75.^\circ8 \pm 2.^\circ8$ to $72.^\circ3 \pm 1.^\circ5$. We conclude that the variation in $l_0$ with distance is real.

### 4.2. *The Local Curvature of the Field Lines*

This change of direction $l_0$ with distance is expected if the field lines are curved. We again return to the railroad tracks, this time standing on the outside of a curve with several sets of tracks, all with the same center of curvature. The direc-

TABLE 2

RESULTS VERSUS DISTANCE, $|b| < 12^\circ$

| Quadrant | ⟨Distance⟩ (kpc) | $\langle A_V \rangle$ (mag) | $l_0$ | $b_0$ | $p_\perp$ | $\sigma^2$ | $N$ |
|---|---|---|---|---|---|---|---|
| 3 ..... | −1.6[a] | 1.3 | $78.7 \pm 5.7$ | $2.1 \pm 2.5$ | $2.50 \pm 0.39$ | 2.92 | 73 |
| 1, near..... | 0.8 | 1.7 | $84.8 \pm 2.5$ | $1.0 \pm 1.4$ | $3.27 \pm 0.40$ | 3.28 | 141 |
| 1, mid ..... | 1.5 | 2.3 | $75.8 \pm 2.8$[b] | $0.8 \pm 0.8$[b] | $4.37 \pm 0.21$ | 2.92 | 313 |
| 1, far..... | 3.1 | 2.0 | $72.3 \pm 1.5$ | $0.0 \pm 0.6$ | $4.46 \pm 0.13$ | 3.00 | 407 |

[a] For quadrant 3 we quote a negative distance, as used in the fit to eq. (7).

[b] For the middle distance range, $\sigma^2$ versus $l_0$ had a double minimum. The $l_0$ and $b_0$ quoted are the averages of the values at the two minima. The two solutions are: $(l_0, b_0) = (72.^\circ7, 1.^\circ1)$ and $(78.^\circ9, 0.^\circ5)$.

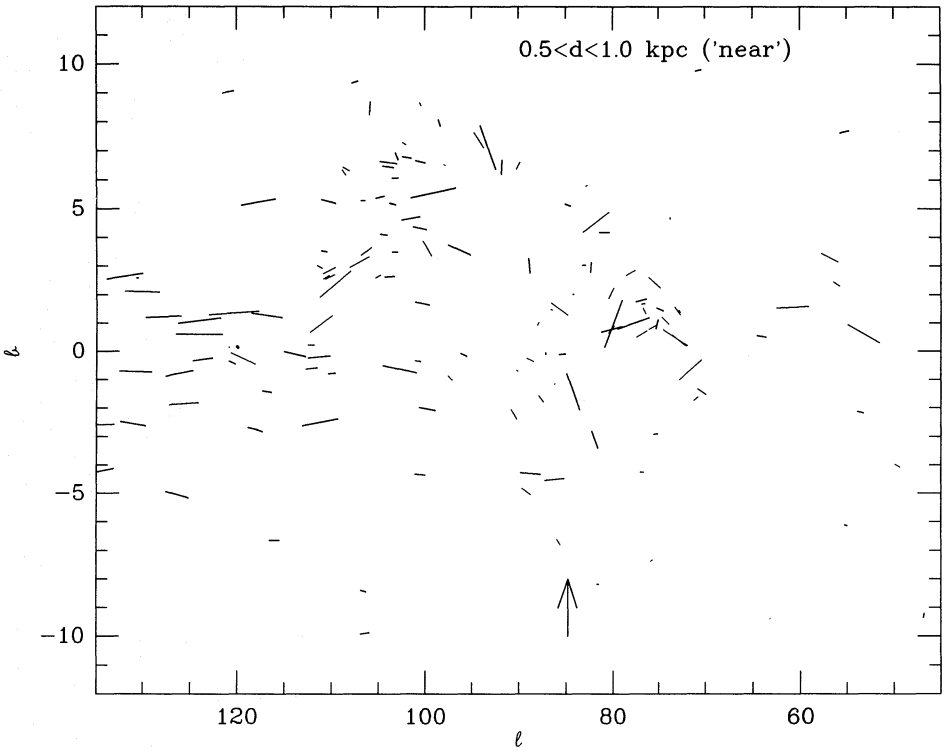


FIG. 3*a*

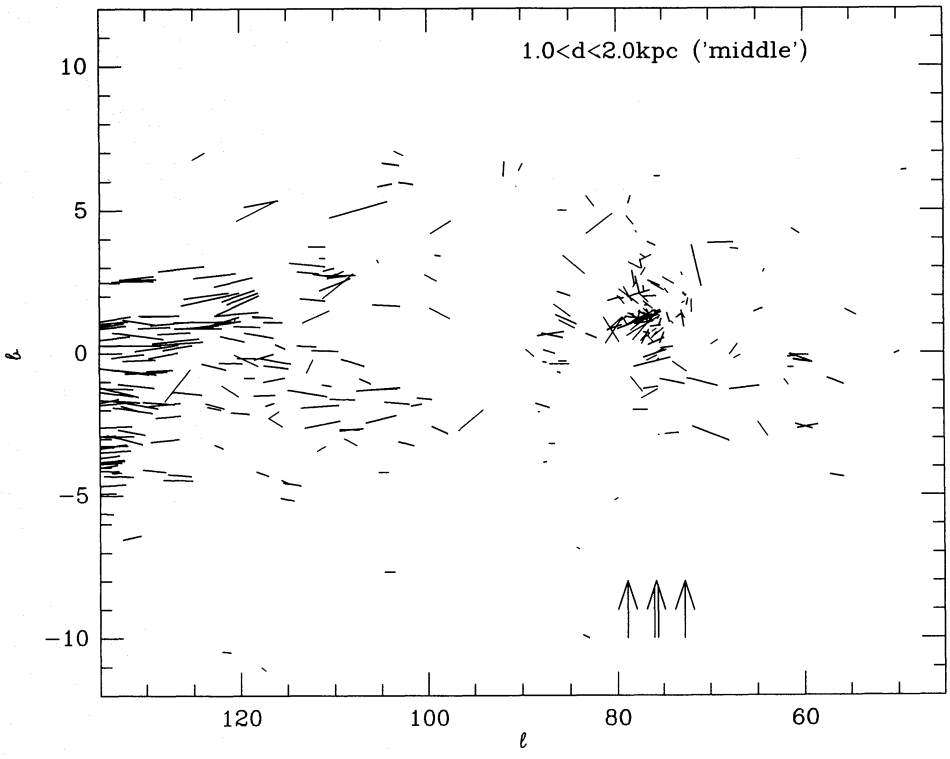


FIG. 3*b*

FIG. 3.—Stellar polarization vectors for our quadrant 1, as in Fig. 1*a*, but binned in distance. The near, middle, and far bins contain 141, 313, and 407 stars, respectively. The arrows show the values of $l_0$ derived from the least-squares fits, as in Fig. 1. See § 4.1.

tion in which the tracks become tangent to the line of sight changes smoothly with distance. In the Galaxy, suppose that the field lines are curved, with the center of curvature located a distance $R_{cc}$ from the Sun in the direction $l_{cc}$. For example, if the center of curvature were the same as the Galactic center, then we would see $\cos l_0 = d/R_{Gal}$, where $d$ is the distance to the tangential point of the field line and $R_{Gal}$ is the Galactoncentric radius of the Sun. In the more general case, we have

$$\cos (l_0 - l_{cc}) = \frac{d}{R_{cc}} . \quad (7)$$

We can use our data to derive both $R_{cc}$ and $l_{cc}$ with a weighted least-squares fit. We consider two different selections of data points: the 4 point solution, which includes all

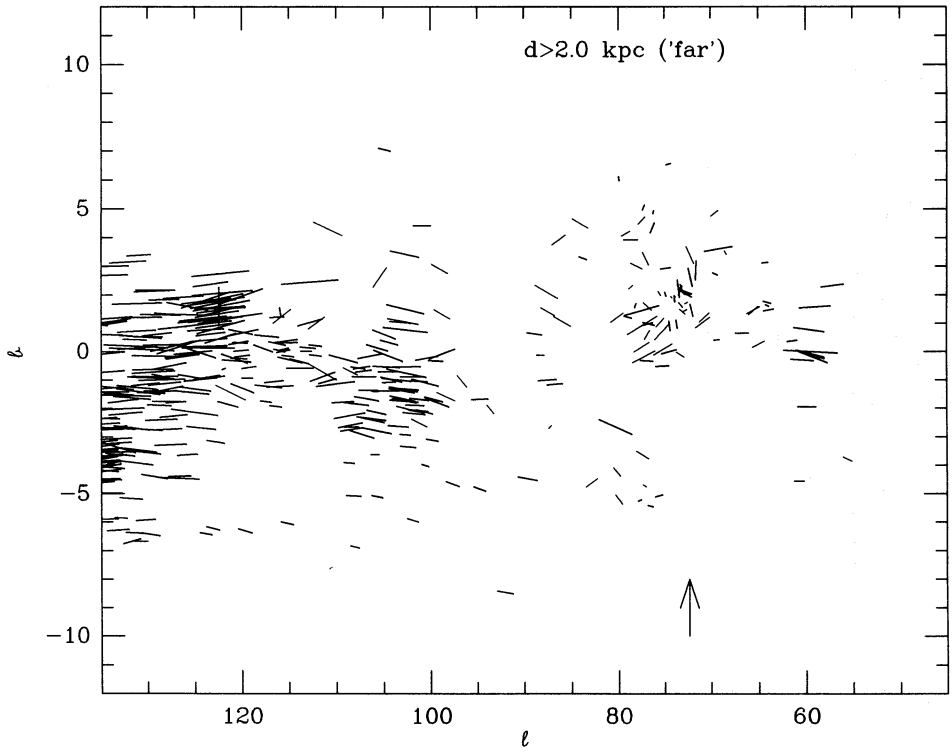


FIG. 3c

four entries in Table 2; and the 3 point solution, which includes only those entries in quadrant 1. For each data point, we assume that the extinction occurs halfway to the mean distance of the stars, and we weight each data point by the inverse square of the uncertainty in $l_0$. We also consider three other assumed cases. These three cases are (1) the "RL pulsar" solution for the local field, with $(R_{cc}, l_{cc}) = (8.5$ kpc, $-2°)$; (2) the "concentric" model for the Galactic field, with $(R_{cc}, l_{cc}) = (8.5$ kpc, $0°)$; and the "spiral-arm" model, for which we adopt the empirical description of Galactic spiral arms as a logarithmic spiral with pitch angle $i = 12°.5$ (This is the mean of the optically determined value [$i = 12°$;

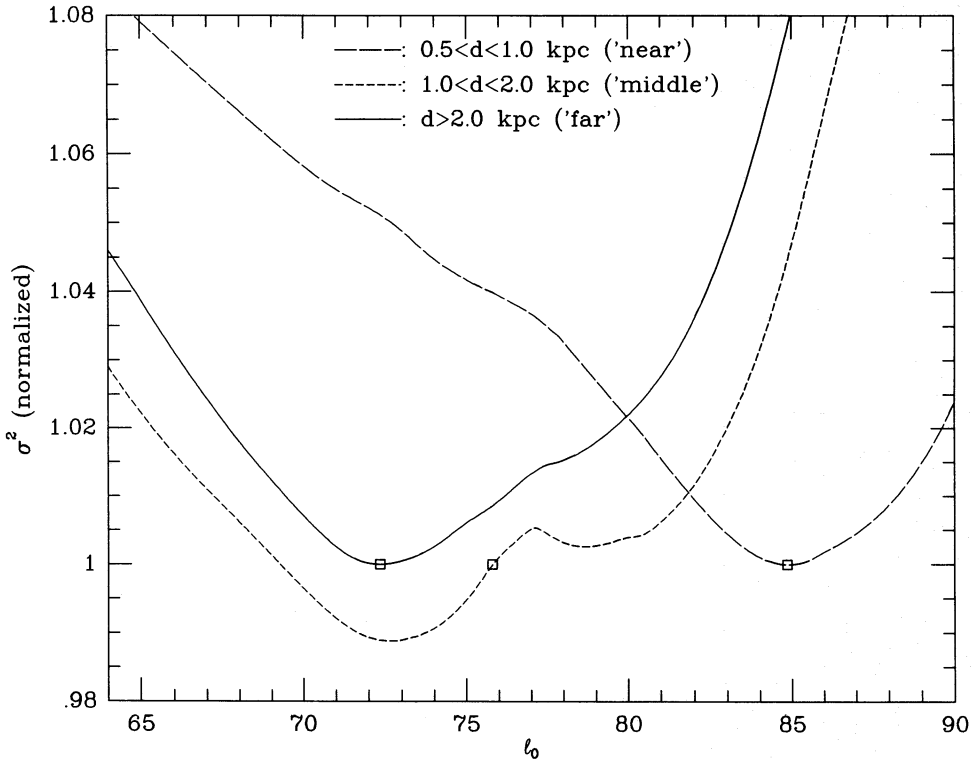


FIG. 4.—Mean square residuals $\sigma^2$ (normalized to their minimum values) vs. $l_0$ for the three distance bins. These solutions include quadrant 1 stars only. See § 4.1 and Table 2.

TABLE 3

STATISTICS FOR MODELS OF FIELD CURVATURE

| Model[a] | $R_{cc}$ (kpc) | $l_{cc}$ | $\chi^2$ | $Q$[b] |
|---|---|---|---|---|
| 4 point fit (eq. [8]) ..... | 8.8 ± 1.8 | −7°.2 ± 4°.1 | 6.4 | 0.042 |
| 3 point fit ..... | 6.0 ± 0.6 | −3°.4 ± 4°.2 | 2.1 | 0.152 |
| RL pulsar (4 point) ..... | 8.5 | −2°.0 | 24.5 | $6.2 \times 10^{-5}$ |
| RL pulsar (3 point) ..... | 8.5 | −2°.0 | 33.5 | $4.2 \times 10^{-4}$ |
| Concentric (4 point)..... | 8.5 | 0°.0 | 41.8 | $1.8 \times 10^{-8}$ |
| Concentric (3 point)..... | 8.5 | 0°.0 | 33.5 | $2.5 \times 10^{-6}$ |
| Spiral-arm (4 point)..... | 8.7 | −12°.5 | 27.8 | $1.4 \times 10^{-5}$ |
| Spiral-arm (3 point)..... | 8.7 | −12°.5 | 27.4 | $5.0 \times 10^{-6}$ |

[a] The first two lines are for the least-squares solutions for $R_{cc}$ and $l_{cc}$ described in § 4.2; the quoted errors are the 1 $\sigma$ errors defined in the usual way, and the number of degrees of freedom of the solutions is 2. The last six lines are for assumed models, so that $R_{cc}$ and $l_{cc}$ have no errors and the number of degrees of freedom is zero.

[b] $Q$ is the formal probability that the model is consistent with the data.

Georgelin & Georgelin 1976] and the radio-determined value [$i = 13°$; Beuermann, Kanbach, & Berkhuijsen 1985].) For a logarithmic spiral, $R_{cc} = R_{Gal}/\cos i$.

Table 3 presents the derived ($R_{cc}$, $l_{cc}$) for our two solutions and also values for the three assumed cases. The table also shows the $\chi^2$ of the fit or the assumed case and the formal probability $Q$ that the fit or the assumed case is consistent with the data (eq. [14.2.12] of Press et al. 1989). We computed $\chi^2$ by taking the $\sigma$ for each point equal to $\sigma_{l_0}$, the error in $l_0$ from Table 2. For the 4 point and 3 point entries, the number of degrees of freedom is 2; they are, of course, $R_{cc}$ and $l_{cc}$. For the assumed cases, the number of degrees of freedom is zero.

Figure 5 shows our two solutions and also the two best of the three assumed cases as lines, together with the four data points from Table 2. The RL pulsar case and the spiral-arm case produce lines that lie quite far from the data points; these models are visually unacceptable, and this is underscored by the low values of $Q$ in Table 3. Our 4 point fit lies about halfway between these two and is moderately acceptable, with its line intersecting two of the four error bars and with $Q = 0.04$. The 3 point fit is more acceptable from the formal standpoint, with the line intersecting two of the three error bars and with $Q = 0.15$. Both the 3 point and the 4 point fits are at least moderately acceptable from the standpoints of both formal statistics and visual inspection.

The interpretation of these results is not well defined, because the number of points is small and the quality of the fit is somewhat disappointing. We offer the following comments:

1. Neither the RL pulsar solution nor the spiral-arm solution is acceptable from the standpoints of both formal statistics and visual inspection.

2. The 4 point fit is somewhat acceptable. Its nonintersection with the error bar of the quadrant 3 point is disappointing because the quadrant 3 stars provide a point with a long "lever arm" in the fit. Unfortunately, this error bar is large because of the small number of stars. If we knew for certain that the fit was inconsistent with this point, then we could conclude that the field lines have variable curvature near the Sun.

3. The 3 point fit is formally more acceptable than the 4 point fit. However, the difference in acceptability is not significant, even with the factor of 3 difference in $Q$, because both fits lie within the realm of acceptability.

4. As we discussed in § 1 above, the random component of the field is large compared to the systematic component and exists over a range of scale length. Furthermore, the

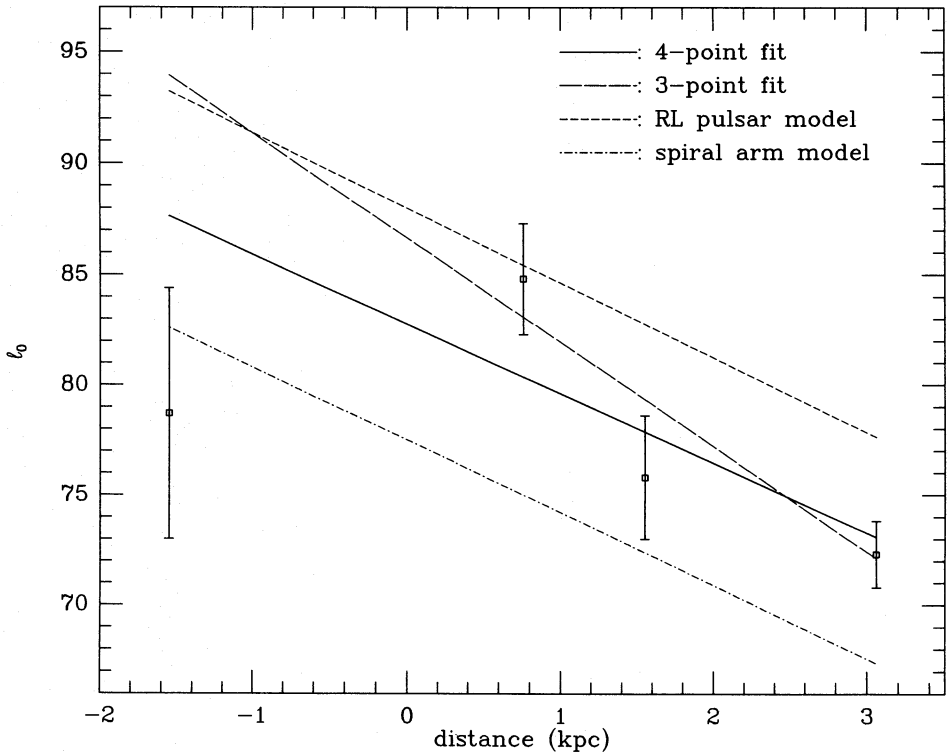


FIG. 5.—Squares with error bars are the solutions for $l_0$ for the four distance bins in Table 2. The solid line, our preferred solution, is our 4 point least-squares fit to these points and has ($R_{cc}$, $l_{cc}$) = (8.8 kpc, −7°.2). The long-dashed line is our 3 point fit with ($R_{cc}$, $l_{cc}$) = (6.0 kpc, −3°.4); the short-dashed line is the RL pulsar solution for the local field with ($R_{cc}$, $l_{cc}$) = (8.5 kpc, −2°.0); the short-dash–long-dash line is the standard Galactic spiral-arm model with ($R_{cc}$, $l_{cc}$) = (8.7 kpc, −12°.5). Table 3 presents the formal statistical acceptabilities of these solutions. See § 4.2.

"far" stars of Table 2 lie beyond the large-scale reversal of the Galactic field that occurs a few hundred parsecs inside the solar circle. In our opinion, the most reasonable interpretation of our results is that the field fluctuates over the scale sampled by the different points in Table 3. Thus, in quadrant 1 $R_{cc}$ decreases and $l_{cc}$ becomes closer to 0°. Because of this "cosmic scatter," we favor the solution that involves the most data from the largest region, even though the formal quality of the fit is less good. Therefore, we adopt the 4 point fit,

$$(R_{cc}, l_{cc}) = (8.8 \pm 1.8 \text{ kpc}, -7.^{\circ}2 \pm 4.^{\circ}1) . \quad (8)$$

The errors, which come directly from Table 3, seem reasonable in light of the above discussion.

## 5. DISCUSSION

### 5.1. *Direction of the Local Field Assuming No Curvature: Pulsars versus Stars*

For the local Galactic field assuming zero curvature, our $l_0$ (§ 3) differs by 10.°6 from RL's pulsar-derived direction 88° ± 5°. We first consider whether this difference is statistically significant. The difference is 2.1 times larger than RL's 1 $\sigma$ error, which makes the agreement somewhat acceptable: the formal probability that our result, 77.°2, is consistent with their result is 0.036.

More telling is the accuracy of our result. The difference is 6 $\sigma_{l_0}$, which formally makes the agreement (almost) impossibly poor. However, the starlight data provide two minima in $\sigma^2$, and this by itself is cause to doubt the significance of the formal error. Although we showed above that this double minimum results from curvature of the Galactic field, we temporarily ignore this result and discuss the agreement as if the double minimum had no apparent cause.

For this discussion, consider the behavior of $\sigma^2$ versus $l$ shown in Figure 2. Clearly, $\sigma^2$ has a well-defined double minimum and the $\sigma^2$ at RL's $l = 88°$ is distinctly much higher than the minimum $\sigma^2$. If one wished, nevertheless, to accept the pulsar solution in favor of ours by allowing such large deviations from the best fit, then one must also accept the fact that it would be preferable to allow *smaller* values of $l$ than our $l_0$ than our $l_0 = 77.^{\circ}4$, because the curvature is smaller toward decreasing $l$. This points again toward the conclusion that the solutions for field direction from the starlight and pulsar data are statistically inconsistent.

If the two results are inconsistent, then which result is more reliable? In our opinion, starlight polarization data are better for deriving the direction of the local field. There are two reasons for this. First, the *random* errors should be smaller, simply because there are many more stars (807) than pulsars (77) in the fits. This is important because of the large "cosmic scatter," which occurs because the random component of the field is so large (§ 1); the larger the number of data points, the better.

Perhaps more important, *systematic* errors should be smaller for the starlight solution, because it is less sensitive to the actual magnetic perturbations that we know, observationally, exist near the Sun. The field direction derived from the starlight data is most responsive to stars located toward the direction the field points. In these directions, there are no obvious magnetic perturbations.

In contrast, the field direction derived from the pulsar data is most responsive to the directions perpendicular to the field, where the pulsar RM's change sign. As an illustration of this point, we note that RL judiciously discard 15 pulsars within 5° of these directions because these pulsars bias the solution too much. Furthermore, toward the inner Galaxy there are two problems: (1) the NPS and (2) the large-scale reversal in the Galactic field that occurs just 0.4 kpc inside of the solar circle. Even though the NPS is so recognizable in the starlight data that we would never dare to include stars behind it, RL do *not* discard pulsars that lie behind it—although, surprisingly, they find that their best-fit direction is not very much affected by them. It is not clear how RL deal with the 0.4 kpc distant reversal. It seems to us that it would be preferable to avoid possible problems with the NPS and the reversal by excluding all pulsars toward the Galactic interior, but, on the other hand, this is one of the two directions to which the fit is most sensitive and excluding these pulsars would be equivalent to discarding half of the information.

We conclude that the accidental circumstances of the location of the Sun with respect to known magnetic perturbations, together with the larger sample of stars, makes the starlight solution preferable to the pulsar solution.

### 5.2. *The Local Field Including Curvature: Our Results in the Context of Other Galaxies*

Section 4.2 shows that our results are inconsistent with the RL pulsar solution, which has the center of curvature of the field lines near the Galactic center; they are even more inconsistent with concentric field lines. Our best estimate is that the center of curvature is located as given in equation (8). The implication is that the field lines are spirals, not circles, because it is almost inconceivable that Galactic field lines are circles that are not concentric with the Galactic center. The local pitch angle of the magnetic lines is $i = 7.^{\circ}2 \pm 4.^{\circ}1$. Even though the formal error is large, our discussion of Table 3 (§ 4.2) shows that the local field lines do not follow the standard Galactic spiral arms with $i \sim 12.^{\circ}5$.

The local field lines might not follow the Galactic spiral arms because the MF data sample primarily the *interarm* magnetic field. This is shown clearly in Figure 5 of Taylor & Cordes (1993), which presents an updated version of the spiral arms found by Georgelin & Georgelin (1976). In models of the Galactic density wave, both the gas and the field are compressed upon entering the shock at the inside of a spiral arm. This causes the gas streamlines and the magnetic field lines to become nearly parallel to the spiral arm inside the arm, while outside the arms they are more nearly concentric circles (Roberts 1969; Roberts & Yuan 1970). This is the proper sense to explain the fact that our derived inclination angle for the interarm field lines is smaller than that of the spiral arms.

However, this explanation does not seem to apply to other spiral galaxies. Not a single external galaxy convincing evidence for variation of inclination angle of the field lines between arm and interarm regions. Particularly good examples are M51 (Neininger 1992) and M83 (Neininger et al. 1991). Although one external galaxy did appear to exhibit such variation, NGC 6946 (Ehle & Beck 1993, Fig. 14), newer observations with higher angular resolution indicate otherwise (Beck 1995).

It would be more philosophically satisfying if the Galaxy were not unique regarding the pattern of its field lines. For external galaxies the field lines have the same inclination as the spiral arms, which makes our result, which finds a difference between these inclination angles, disturbing. We

believe that there are only two ways to rationalize the incompatibility with external galaxies. One is, of course, to invoke observational error either in the present paper or in the standard model of Galactic spiral arms. The other is to invoke local distortion in the spiral structure or the magnetic field lines; in external galaxies, the field lines follow local distortions of the arms closely (e.g., Neininger et al. 1991). This distortion may occur on a Galactic scale—for example, being related to the field reversal that lies 0.4 kpc inside the solar circle (RL)—or it may occur on smaller scales. A third possible alternative explanation fails: it invokes the fact that in our analysis the distances to the stars are known but the distances to the extinction are not; we have assumed the extinction occurs halfway to the stars. However, this affects only $R_{cc}$ but not the inclination.

## 6. SUMMARY

We have used MF's compilation of starlight polarization data to derive the local direction and curvature of the Galactic magnetic field lines. If we assume that the field lines have no curvature, then they point toward $(l_0, b_0) = (77\overset{\circ}{.}4 \pm 1\overset{\circ}{.}8, 0\overset{\circ}{.}4 \pm 0\overset{\circ}{.}5)$ (eq. [6]). However, in § 4 we show that the curvature is reliably detected, with the local field lines pointing toward $l_0 = 82\overset{\circ}{.}8 \pm 4\overset{\circ}{.}1$. In § 4.2 we discuss ambiguities of the interpretation of our results and settle on a local distance and direction to the center of curvature $(R_{cc}, l_{cc}) = (8.8 \pm 1.8 \text{ kpc}, -7\overset{\circ}{.}2 \pm 4\overset{\circ}{.}1)$.

Despite these apparently large errors in $R_{cc}$ and $l_{cc}$, we show that with high statistical confidence our results are inconsistent with RL's pulsar result having $(R_{cc}, l_{cc}) = (8.5 \text{ kpc}, -2°)$, with a concentric-circle model having $(R_{cc}, l_{cc}) = (8.5 \text{ kpc}, 0°)$, and with a spiral-arm model having inclination $(R_{cc}, l_{cc}) = (8.7 \text{ kpc}, -12\overset{\circ}{.}5)$ (the standard value for the Galactic spiral arms). In § 5.2 we compare our Galactic results with those for external galaxies, for which the field lines follow the spiral pattern closely. It is difficult to reconcile the two without invoking local distortions of the spiral pattern or the field lines; such distortions might conceivably be Galactic in scale and related to the field reversal that occurs just inside the solar circle.

It is a pleasure to acknowledge comments by Rainer Beck, Richard Rand, and Ellen Zweibel. I am grateful to Don Mathewson, who shipped me the polarization data on punched cards more than 20 years ago; I have religously backed up these data over the years through the evolution of several computer systems. This work was supported in part by an NSF grant to the author.

## REFERENCES

Beck, R. 1993, in IAU Symp. 157, The Cosmic Dynamo, ed. F. Krause, K.-H. Rädler, & G. Rüdiger (Dordrecht: Kluwer) 283
Beck, R. 1995, private communication
Beuermann, K., Kanbach, G., & Berkhuijsen, E. M. 1985, A&A, 153, 17
Bevington, P. R. 1969, Data Reduction and Error Analysis for the Physical Sciences (New York: McGraw-Hill)
Ehle, M., & Beck, R. 1993, A&A, 273, 45
Georgelin, Y. M., & Georgelin, Y. P. 1976, A&A, 49, 57
Heiles, C. 1976, ARA&A, 14, 1
Heiles, C. 1995, in ASP Conf. Ser. 80, The Physics of the Interstellar Medium and Intergalactic Medium, ed. A. Ferrara, C. F. McKee, C. Heiles, & P. R. Shapiro (San Francisco: ASP), 507
Heiles, C. 1966, in ASP Conf. Ser., Polarimetry of the Interstellar Medium, ed. W. G. Roberge & D. C. B. Whittet (San Francisco: ASP), in press
Heiles, C., Chu, Y.-H., Reynolds, R. J., Yegingil, I., & Troland, T. H. 1980, ApJ, 242, 533
Jones, T. J., Klebe, D., & Dickey, J. M. 1992, ApJ, 389, 602
Mathewson, D. S., & Ford, V. L. 1970, MmRAS, 74, 139 (MF)
Neininger, N. 1992, A&A, 263, 30
Neininger, N., Klein, U., Beck, R., & Wielebinski, R. 1991, Nature, 352, 781
Ohno, H., & Shibata, S. 1993, MNRAS, 262, 953
Paresce, F. 1984, AJ, 89, 1022
Press, W. H., Flannery, B. P., Teukolsky, S. A., & Vetterling, W. T. 1989, Numerical Recipes (Cambridge: Cambridge Univ. Press)
Rand, R. J., & Kulkarni, S. R. 1989, ApJ, 343, 760
Rand, R. J., & Lyne, A. G. 1994, MNRAS, 268, 497 (RL)
Roberts, W. W. 1969, ApJ, 158, 123
Roberts, W. W., & Yuan, C. 1970, ApJ, 161, 877
Taylor, J. H., & Cordes, J. M. 1993, ApJ, 411, 674
Vallée, J. P. 1993, ApJ, 419, 670